Fuzzy Single-Current Field Weakening Control of IPMSM in EV

WU Jingbo，LIU Junjie，XIE Chengwei，GUO Zhijun

Abstract—**The driving speed of pure electric vehicles changes frequently under complex driving conditions, and there is no mathematical law to follow. Poor working conditions will lead to varying driving motor parameters. Traditional motor control PI regulator parameters are fixed and cannot be adjusted in real time following the vehicle driving state. The dynamic performance of the drive system decreases due to the increase of AC/DC coupling in the high-speed field weakening region of the interior permanent magnet synchronous motor (IPMSM). To solve the above problems, an IPMSM fuzzy single-current field weakening control algorithm for pure electric vehicles was proposed, and the parameters of the PI regulator were adjusted in real time through fuzzy control to enhance the response characteristics and anti-interference characteristics of the drive system. The optimized single-current field weakening control method was adopted, and the a-axis and d-axis voltage was adjusted in real time based on the vehicle speed and the output torque, which enhanced the control performance of the vehicle in the high-speed field weakening region. The feasibility and effectiveness of the proposed control algorithm were verified through a simulation comparison with the traditional PI-adjusted single-current field weakening control algorithm.**

Keywords—**Pure Electric Vehicle, IPMSM, Field Weakening, Single Current**

I. Introduction

Interior Permanent Magnet Synchronous Motor (IPMSM) is characterized by high power density and excellent torque-speed characteristics, so it shows significant advantages in reliability, high torque density, as well as the realization of field weakening control[1]. Due to abundant rare earth resources in China, IPMSM has been widely applied in the field of pure electric vehicle drive[2,3]. Limited by the inverter DC terminal voltage, the inverter voltage saturation cannot continue to increase the speed when reaching the base speed, so IPMSM should adopt field weakening control technology to increase the speed regulation range of IPMSM without changing the motor structure and inverter capacity[4], which can conform to the high-speed performance requirements of pure electric vehicles.

Manuscript received July 14, 2023; revised October 22, 2023.

WU Jingbo is an associate professor of Henan University of Science and Technology, Luoyang 471000 China. (e-mail: wubocn2005@163.com).

LIU Junjie is an engineer of Geely Automobile Research Institute, Ningbo 315000 China. (e-mail: Junjie.Liu5@geely.com).

XIE Chengwei is a PhD candidate of Henan University of Science and Technology, Luoyang 471000 China. (corresponding author to provide phone: 86-17838915172; e-mail: maruyuet@163.com).

GUO Zhijun is an professor of Henan University of Science and Technology, Luoyang 471000 China. (e-mail: gzhijun1970@163.com).

Extensive studies have been conducted to solve the following problems: the parameters of the traditional PI current regulator are fixed and cannot be adjusted under real-time traffic conditions; both the rapidity and stability of the system cannot be considered in the determination of proportional and integral gain to give attention; the enhancement of the a-axis and d-axis current coupling of the IPMSM in the high-speed field weakening region results in a reduced dynamic performance of the drive system. Literature [5,6] presented a differential feedback control strategy to increase the response speed and the consistent overshoot ability of the system. Literature [7] proposed a PI parameter design rule to achieve the fast control of current without overshooting and enhance the performance of the current loop. In Literature [8], the prediction model of adjacent periods was adopted to eliminate the constant term, thus avoiding over-harmonic oscillation in PI control. In Literature [9], the fuzzy adaptive method was employed to dynamically adjust the approach rate parameters, which increased the response speed of the system compared with the traditional PI. In Literature [10], a field weakening control system of a single-current regulator based on virtual resistance was built for efficiency optimization while ensuring dynamic speed regulation performance and carrying capacity.

In this paper, an IPMSM fuzzy single-current field weakening control algorithm for pure electric vehicles was proposed, and the parameters of the PI regulator were adjusted in real time by fuzzy control to enhance the response characteristics and anti-interference characteristics of the drive system. The optimized single-current field weakening control method was adopted to optimize the a-axis and d-axis current coupling of the motor in the field weakening region and simply the control strategy. The AC axis voltage changed with the vehicle speed and the vehicle output torque in real time, which made the driving motor stable at its optimal operating point, such that the magnetic weakening efficiency and load capacity of the motor increased. By combining fuzzy control with the optimized single current regulator field weakening control strategy, the driving motor of pure electric vehicles can fully exploit the advantages of both and achieve a better control effect in the high-speed field weakening region.

II. IPMSM Mathematical Model

IPMSM is a multi-variable, close-coupling, and nonlinear time-varying complex system. Under certain constraints, its mathematical model can be simplified for research and analysis[11]. Before the mathematical model is built, the following model assumptions are proposed[12]:

Under the assumed conditions, the voltage equation of the IPMSM in steady-state operation in the d-q synchronous rotation coordinate system is expressed as:

$$\left.\begin{aligned} u_{\mathrm{d}} &= R_{\mathrm{s}} i_{\mathrm{d}} + L_{\mathrm{d}} \frac{\mathrm{d}i_{\mathrm{d}}}{\mathrm{d}t} - L_{\mathrm{q}} \omega_{\mathrm{e}} i_{\mathrm{q}} \\ u_{\mathrm{q}} &= R_{\mathrm{s}} i_{\mathrm{q}} + L_{\mathrm{q}} \frac{\mathrm{d}i_{\mathrm{q}}}{\mathrm{d}t} + L_{\mathrm{d}} \omega_{\mathrm{e}} i_{\mathrm{d}} + \omega_{\mathrm{e}} \psi_{\mathrm{f}} \end{aligned}\right\} \tag{1}$$

The stator flux equation is written as:

$$\left.\begin{aligned} \psi_{\mathrm{d}} &= L_{\mathrm{d}} i_{\mathrm{d}} + \psi_{\mathrm{f}} \\ \psi_{\mathrm{q}} &= L_{\mathrm{q}} i_{\mathrm{q}} \end{aligned}\right\} \tag{2}$$

In Eqs. (1) and (2), u_{d} and u_{q} denote the components of the stator voltage on axes d and q; id and i_{q} represent the components of the stator current on axes d and axis q, respectively. L_{d} and L_{q} represent the inductance of axis d and axis q, respectively. ψ_{d} and ψ_{q} expresses the components of the stator flux along axis d and axis q, respectively. R_{s} denotes the stator resistance of the motor; ψ_{f} is the permanent magnet flux; ω_{e} is the electric angular velocity of the rotor.

When IPMSM runs at high speeds, if the effect of its stator resistance Rs is ignored, the steady-state voltage equation of the motor in the d-q synchronous rotation coordinate system can be expressed as:

$$\left.\begin{aligned} u_{\mathrm{d}} &= -L_{\mathrm{q}} \omega_{\mathrm{e}} i_{\mathrm{q}} \\ u_{\mathrm{q}} &= \omega_{\mathrm{e}} \left(L_{\mathrm{d}} i_{\mathrm{d}} + \psi_{\mathrm{f}} \right) \end{aligned}\right\} \tag{3}$$

The electromagnetic torque equation of the motor is written as:

$$T_{\mathrm{e}} = \frac{3}{2} p_{\mathrm{n}} i_{\mathrm{q}} \left[i_{\mathrm{d}} \left(L_{\mathrm{d}} - L_{\mathrm{q}} \right) + \psi_{\mathrm{f}} \right] \tag{4}$$

Where T_{e} denotes the electromagnetic torque; p_{n} represents the polar logarithm of the motor.

The direct axis inductance of the IPMSM is smaller than the cross-axis inductance, and its electromagnetic torque T_{e} comprises the permanent magnet torque Tr generated by the interaction between the rotor permanent magnet and the stator air gap magnetic field and the reluctance torque Tm generated by the convex pole effect, which is expressed as follows:

$$\left.\begin{aligned} T_{\mathrm{r}} &= \frac{3}{2} p_{\mathrm{n}} i_{\mathrm{q}} \psi_{\mathrm{f}} \\ T_{\mathrm{m}} &= \frac{3}{2} p_{\mathrm{n}} i_{\mathrm{q}} i_{\mathrm{d}} \left(L_{\mathrm{d}} - L_{\mathrm{q}} \right) \end{aligned}\right\} \tag{5}$$

III. Operation constraints of IPMSM and field weakening control principle

A. Operation constraints of IPMSM

The inverter transforms the DC current of the power battery into the AC current of the driving motor. IPMSM is limited by the output capacity of the inverter and the capacity of the motor during operation. Besides, there are voltage and current constraints, i.e., the stator current vector of the motor should meet the voltage limit equation and current limit equation.

Voltage constraints

In steady-state operation, the input voltage of IPMSM is limited by the DC side voltage of the inverter and the insulation level of the motor. If the stator voltage is extremely high, the insulation layer will be broken down, and the motor will be damaged [13]. The limit value u_{smax} of the voltage resultant vector us of the stator end of the driving motor is correlated with the DC side voltage u_{dc} of the inverter and the PWM modulation algorithm. In this paper, the SVPWM modulation algorithm with higher voltage utilization rate was adopted, $u_{\mathrm{smax}} = u_{\mathrm{dc}} / \sqrt{3}$, and the voltage limiting equation is expressed as:

$$u_{\mathrm{d}}^{\ 2} + u_{\mathrm{q}}^{\ 2} = u_{\mathrm{s}}^{\ 2} \le u_{\mathrm{smax}}^{\ 2} \tag{6}$$

Substituting Eq. (3) into Eq. (6), the voltage limit equation is defined as:

$$\left(L_{\mathrm{q}} i_{\mathrm{q}} \right)^2 + \left(L_{\mathrm{d}} i_{\mathrm{d}} + \psi_{\mathrm{f}} \right)^2 \le \frac{u_{\mathrm{smax}}^{\ 2}}{\omega_{\mathrm{e}}} \tag{7}$$

In the i_{d}-i_{q} coordinate system, the voltage limit equation curve is a family of ellipses with a center of , termed the voltage limit ellipse. With the increase of the speed, the ellipse contracts, as presented in Fig. 1.

Current constraints

The amplitude of the stator current resultant vector is of the IPMSM should not exceed the upper limit of the current of the power device i_{smax}. The current limiting equation is written as:

$$i_{\mathrm{d}}^{\ 2} + i_{\mathrm{q}}^{\ 2} = i_{\mathrm{s}}^{\ 2} \le i_{\mathrm{smax}}^{\ 2} \tag{8}$$

The motor stator current limit equation curve is a circular track with a center point of (0,0) in the i_{d}-i_{q} coordinate system, which is termed the current limit circle, as presented in Fig. 1.

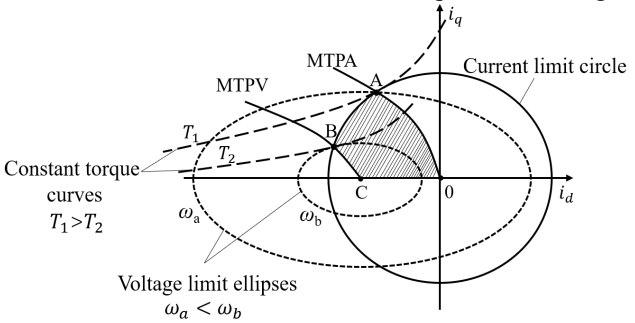

Fig. 1. Field magnetic control voltage and current vector trajectory of IPMSM

B. Principle of field weakening speed expansion of IPMSM

By substituting stator flux $\psi_{\mathrm{s}} = \sqrt{\psi_{\mathrm{q}}^{\ 2} + \psi_{\mathrm{d}}^{\ 2}}$ into Eq. (7), the correlation between stator flux, electric angular velocity, and

voltage limit value of IPMSM is expressed as:

$$\psi_s \cdot \omega_e \le u_{smax} \tag{9}$$

$$\psi_s = \sqrt{\left(L_d i_d + \psi_f\right)^2 + \left(L_q i_q\right)^2} \tag{10}$$

Based on Eq. (9), as the motor speed increases, the amplitude of the stator voltage constantly increases, and the output voltage of the inverter reaches the maximum when it reaches the base speed. Eq. (10) suggests that the speed can only be continuously increased by adjusting id and i_q. In the motor driving process, the motor stator current is in the second quadrant, as shown in Fig. 1. As depicted in this figure, id is negative and i_q is positive. The basic principle of field weakening control is appropriately adjusting the distribution relationship between i_d and i_q in the stator-voltage restricted state[14]. Below the base speed, pure electric vehicles generally use the Max Torque Per Ampere (MTPA) control algorithm to make the drive motor run in the constant-torque region. Accordingly, under the given load torque, the stator current of the motor is minimal, the energy loss is reduced, and the vehicle range increases[15]. Fig. 1 illustrates the MTPA curve. Above the base speed, the motor runs in the field weakening region, and the stator current is on the AB and BC curves in Fig. 1 or in the shaded area. The MTPV (Max Torque Per Voltage) curve in Fig. 1 represents the current track corresponding to the maximum electromagnetic torque that the motor can output at different speeds, which ensures that the vehicle possesses the capability of outputting a large torque at high speeds. In the field weakening region, the numerical size and change direction of id and iq are allocated by the control algorithm to weaken the air gap magnetic field and increase the motor speed range.

IV. Optimized Single-Current Regulator

An optimized single-current regulator field weakening control algorithm was adopted in this paper to solve the a-axis and d-axis current coupling problem caused by the field weakening control mode of the traditional IPMSM dual-current regulator. In the vehicle driving process, the vehicle output torque from the vehicle driving system was calculated by the VCU to obtain the electromagnetic torque T_e of the motor at the moment. With the given current i_q*, the given current i_d* can be calculated by Eq. (4). The a-axis and d-axis voltage instruction of the driving motor can be adjusted in real time with the change in the speed and the output torque of the vehicle. Fig. 2 depicts the block diagram of field weakening control based on MTPA and optimized single current regulator. the proposed field weakening control strategy is characterized by a simple structure and easy implementation, fast dynamic response, and good robustness as compared with the traditional field weakening control strategy based on a double current regulator.

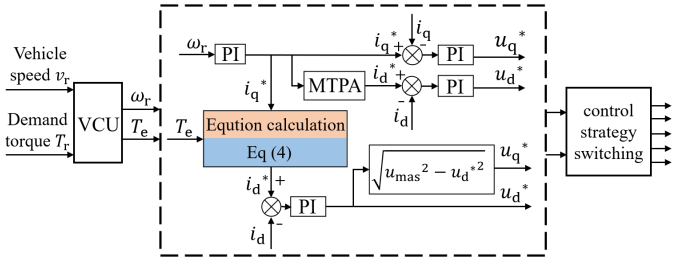

Fig. 2. Block diagram of MTPA and optimized single-current field weakening control

The voltage of the power battery of pure electric vehicles will decrease with the loss of energy. With voltage saturation as the switching condition of the control strategy, the motor will enter the field weakening area in advance, and the speed regulation range will decrease[16,17]. In this paper, the correlation between motor speed and base speed value served as the switching condition of the control mode, as presented in Fig. 3.

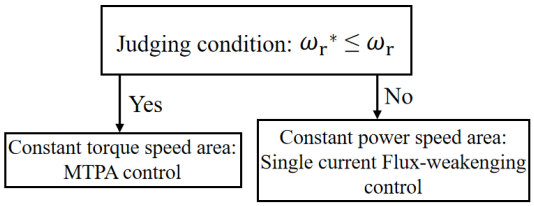

Fig. 3. Control mode switching conditions

V. Design of Fuzzy-PI

IPMSM is characterized by nonlinear, strong coupling, and parameter change in high-speed operation, and the motor parameters may change when the vehicle is driven under bad road conditions. The traditional PI regulator with constant gains is designed following the exact mathematical model of the motor and is still within the range of linear control, thus resulting in a situation where neither the dynamic response characteristic nor the anti-interference characteristic can reach the ideal state [18,19]. When applying the fuzzy control theory to the traditional PI regulator, the motor drive system can adjust the parameters of the PI regulator in real time to achieve the desired control effect by exploiting its strong system adaptability, robustness, and fault tolerance.

The deviation e and the deviation change rate e_c of the expected value and the feedback value of the motor speed are taken as the inputs of the fuzzy controller. Based on the fuzzy knowledge base (control rules and membership function), fuzzy reasoning and anti-fuzzy are conducted to determine the online adjustment changes ΔK_p and ΔKi of the PI regulator parameters K_p and K_i. The synchronous change values K_p* and K_i* are obtained after correction from Eq. (11), which are introduced to the calculation of the control system. The fuzzy PI control block diagram of the IPMSM drive system is illustrated in Fig. 4. The online correction relationship of Ki*and Ki is defined as follows:

$$\left.\begin{aligned} K_p^* &= K_p + \Delta K_p \\ K_i^* &= K_i + \Delta K_i \end{aligned}\right\} \tag{11}$$

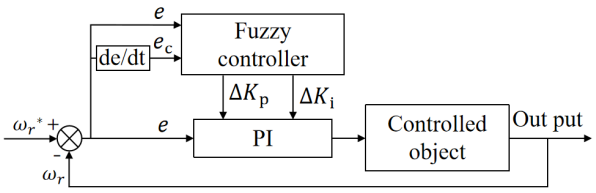

Fig. 4. Fuzzy PI block diagram

After the fuzzification of the speed deviation e and its rate change e_c, the corresponding fuzzy variables are E and E_c, which are the input of the controller. The fuzzy quantity Up and Ui corresponding to ΔK_p and ΔKi are the output of the controller. Their fuzzy subset is set as {NB, NM, NS, ZO, PS, PM, PB}; The domain interval of the input and output variables is set as [-3, 3]. The triangular membership function with less computation, saving storage space, and high sensitivity serves as the membership function of the input-output fuzzy quantity.

The control rule table of the fuzzy controller is established, as shown in Tables 1 and 2.

TABLE I
TABLE OF ΔKP FUZZY CONTROL RULES

ΔK_p	e_c	NB	NM	NS	ZO	PS	PM	PB
	NB	PB	PB	PM	PM	PS	PS	ZO
	NM	PB	PM	PM	PS	PS	ZO	NS
	NS	PM	PS	PS	PS	ZO	NS	NM
e	ZO	PB	PM	PS	ZO	PS	PM	PB
	PS	NM	NS	ZO	PS	PS	PS	PM
	PM	NS	ZO	PS	PS	PM	PM	PB
	PB	ZO	PS	PS	PM	PM	PB	PB

TABLE II
TABLE OF ΔKI FUZZY CONTROL RULES

ΔK_p	e_c	NB	NM	NS	ZO	PS	PM	PB
	NB	PB	PB	PM	PM	NS	NM	NB
	NM	PB	PB	PM	PM	PS	NS	NM
	NS	PB	PB	PM	PS	ZO	NS	NM
e	ZO	PB	PM	PS	ZO	PS	PM	PB
	PS	NM	NS	ZO	PS	PM	PB	PB
	PM	NM	NS	PS	PM	PM	PB	PB
	PB	NB	NB	NS	PM	PM	PB	PB

After the tables of control rules are established, the Mamdani fuzzy reasoning method is used for reasoning, and the reasoning process is illustrated in Fig. 5.

The data obtained by employing the Mamdani reasoning method should be defuzzied to obtain the exact output variables. Due to the limitation of accuracy, the center of gravity method is adopted to solve the fuzzy problem, which is formulated in the following function form:

$$z_0 = \left(\sum_{i=1}^{n} \mu C'(z_i) \cdot z_i \right) / \sum_{i=1}^{n} \mu C'(z_i) \tag{12}$$

Where z0 denotes the exact value of the output control quantity after solving the fuzzy problem, zi represents the output fuzzy variable, and is the membership function of zi.

In brief, the block diagram of the fuzzy single-current field weakening control system of IPMSM for pure electric vehicles is presented in Fig. 6.

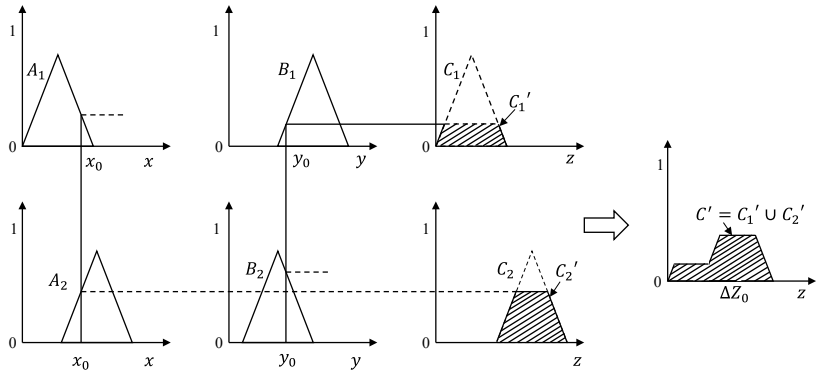

Fig. 5. Mamdani reasoning process

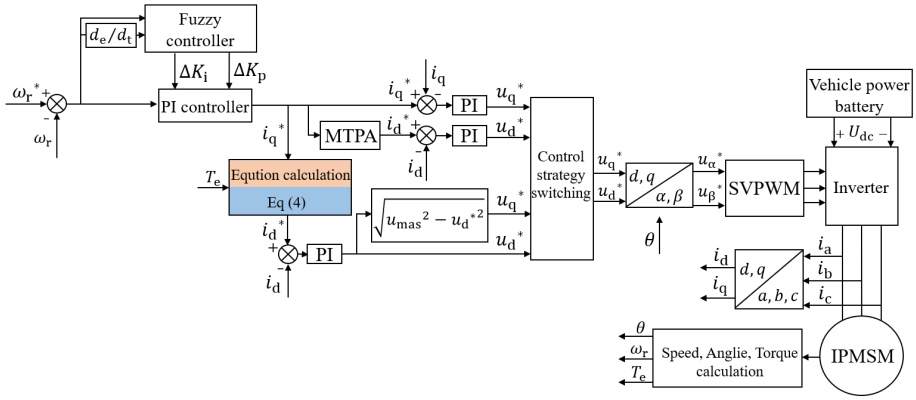

Fig. 6. Block diagram of the IPMSM fuzzy single-current field weakening control system for pure electric vehicles

VI. Simulated Analysis

The simulation model based on Fig. 6 was built in Matlab/Simulink, and then the results were compared and analyzed with the traditional PI-adjusted single-current field weakening control algorithm under the same simulation parameters and operating conditions. The simulation parameters of the IPMSM are listed in Table 3.

TABLE III
Simulation Parameters

Parameter	Value
Stator resistance R/Ω	0.24
d-axis inductance L_d/mH	18
q-axis inductance L_q/mH	36
Permanent magnet flux linkage ψ_f/Wb	0.009
Polar logarithm P_n per unit	6
Rotational inertia J/(kg·m2)	0.00015
dc-side voltage Vdc/V	75
Motor base speed value n/（r/min）	4000

The simulation duration was 0.3s, and three working conditions (constant speed, speed step, and load disturbance) were selected for the simulation test. Moreover, the motor speed curve, a-axis and d-axis current curve, and electromagnetic torque curve were observed and analyzed in a Simulink Date Inspector.

Figs. 7(a) and 7(b) depict the speed curves of the IPMSM fuzzy single-current field weakening control algorithm (the proposed control algorithm) and the traditional PI-adjusted single-current field weakening control algorithm (the traditional control algorithm) under the condition that the motor was no-load and there was a given constant input target speed of 3000rpm. both can quickly respond to the target speed value of 3000rpm without overshooting.

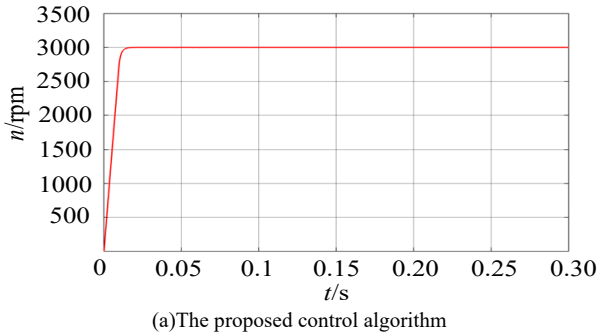

(a)The proposed control algorithm

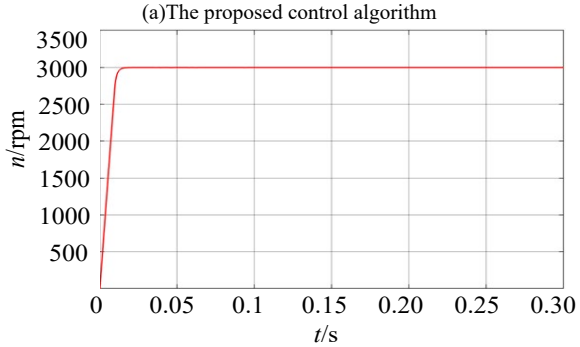

(b) Traditional control algorithm

Fig. 7. Simulation curve of rotation speed

The motor was provided with a speed input signal of 4000rpm to 8500rpm in 0.1s step.

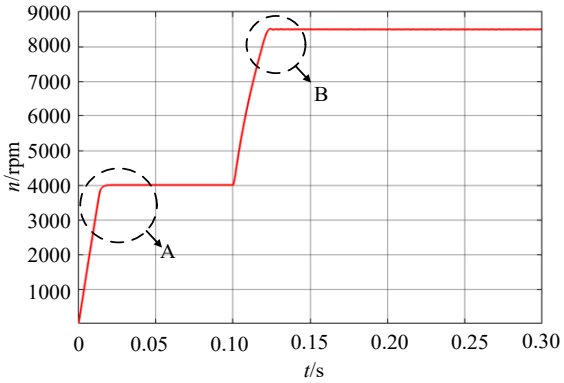

(a)Overall diagram of speed simulation curve of the proposed control algorithm

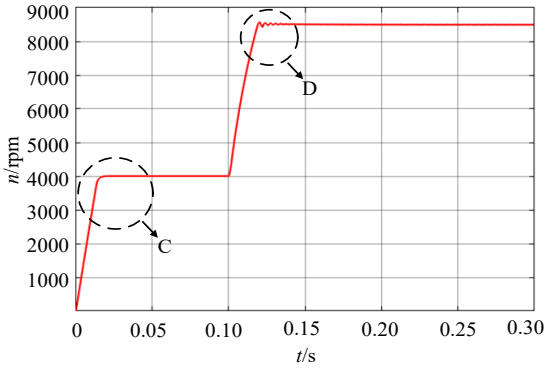

(b) Overall diagram of speed simulation curve of the traditional control algorithm

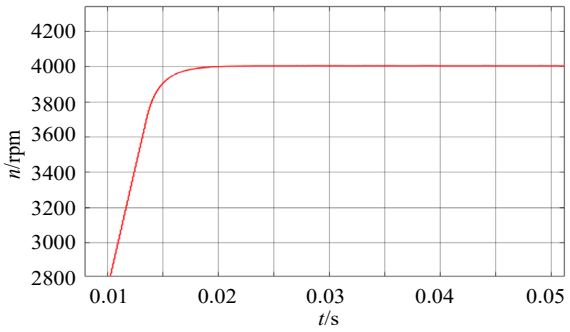

(c) The curve of A

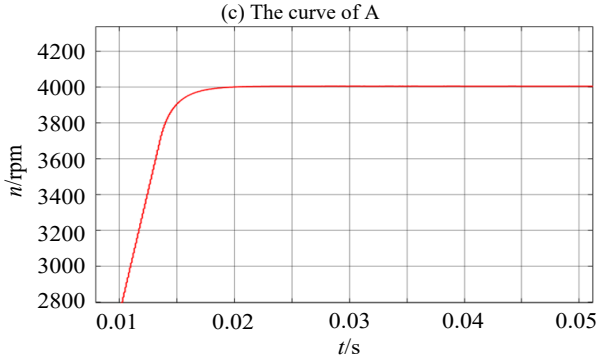

(d) The curve of C

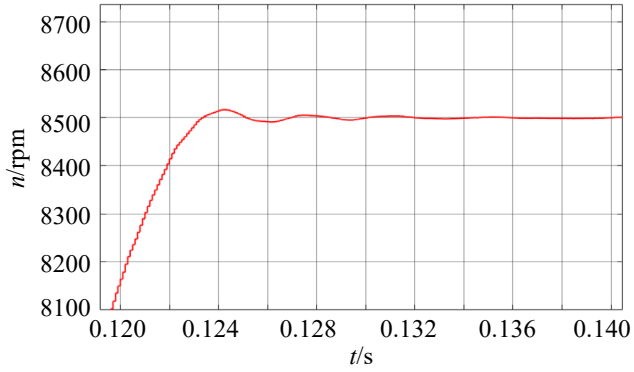

(e) The curve of B

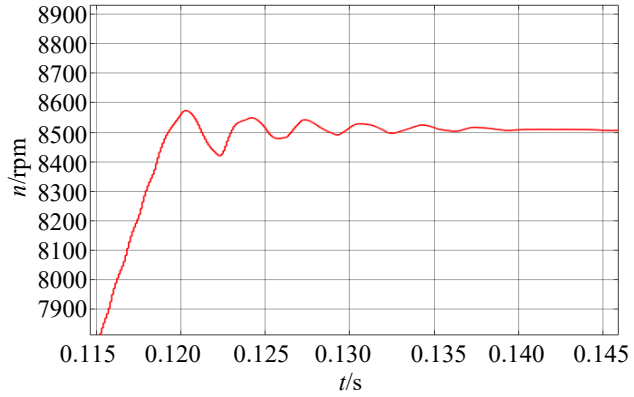

(f) The curve of D

Fig. 8. Overall simulation curve of speed and local enlarged drawing

A and B represent partial enlarged drawings of the speed curve, represented by Figs. (c) and (e), respectively.C and D are partial enlarged drawings of the speed curve, represented by (d) and (f).

Figs. 8(a) and 8(b) depict the overall simulation curves of the speed of the proposed control algorithm and the traditional control algorithm, respectively. The overall curve suggests that both can quickly reach the target speed and follow well. Figs. (c) and (d) depict the partial enlarged drawings of the speed curves of the two control algorithms at the base speed value lower than 4000rpm. As revealed by this result, the two control algorithms had a fast reaction speed to reach the target speed and can be well consistent with the target value. Figs. (e) and (f) depict the partial enlarged drawings of the speed curves of the two control algorithms close to the time at the base speed value higher than 8500rpm. The above comparison revealed that in the field weakening region, the proposed control algorithm had less overshooting and less fluctuation of the speed curve than the traditional method when following the target speed. The former reached the target speed stable value at 0.130s, while the latter reached the target speed stable value at 0.140s. The above result suggested that the proposed control algorithm had smaller overshooting, faster response speed, smaller fluctuation before reaching the stable value and stronger robustness in the field weakening region than the traditional control algorithm.

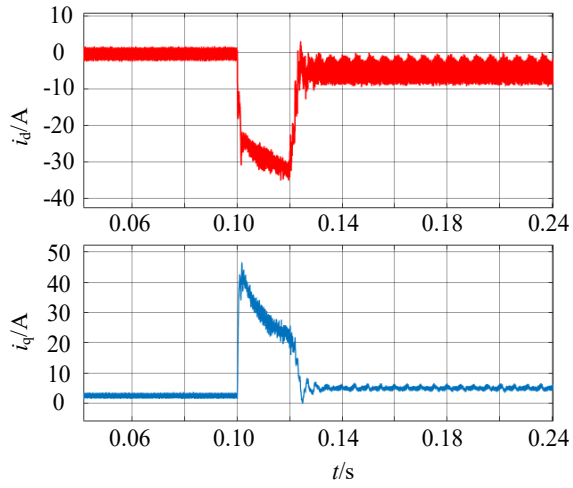

(a)The proposed control method

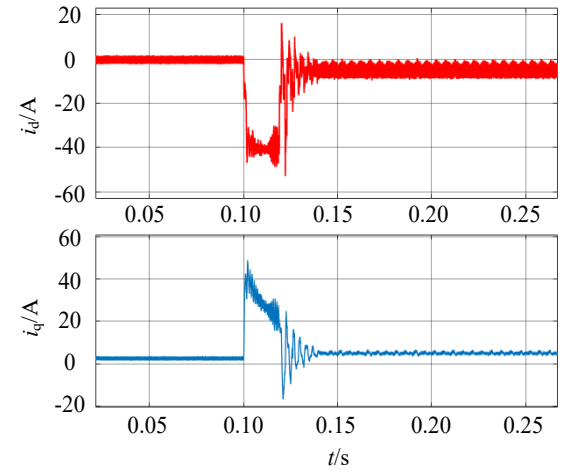

(b) Traditional control method

Fig. 9. A-axis and d-axis current response curves

Figs. 9(a) and 9(b) depict the a-axis and d-axis current response curves of the proposed control algorithm and the traditional control algorithm under the step changes of speed (4000rpm to 8500rpm), respectively. In the field weakening region, the current fluctuation based on the traditional control algorithm was more significant, and the id pulse value was higher. The current curve based on the proposed control algorithm was smoother, the id pulse value was smaller, and i_d and i_q stabilized faster in the field weakening region. The above results suggested that the proposed control algorithm showed more advantages in restraining current disturbance and reducing current coupling in the high-speed field weakening region and possessed strong robustness and adaptability.

2Nm external load torque was added at 0.1s based on the above step change in speed.

As depicted in Figs. 10(a) and 10(b), when the speed and load torque changed simultaneously, the average pulse value of id under the proposed control algorithm was smaller. I_q fluctuated less, and its curve was smoother. A sudden change in motor speed and load torque is conducive to protecting electronic power devices, thus indicating that the proposed control algorithm has excellent anti-interference characteristics.

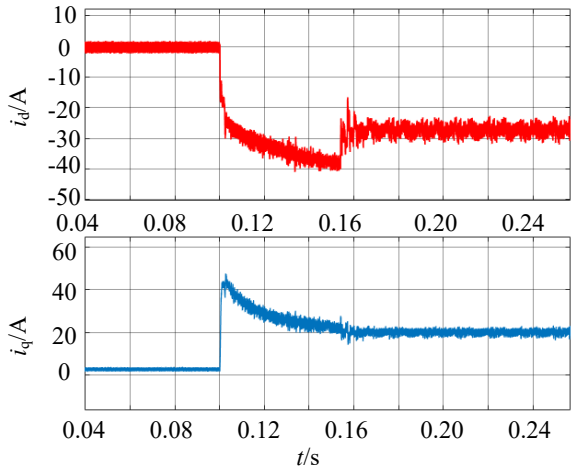

(a) The proposed control method

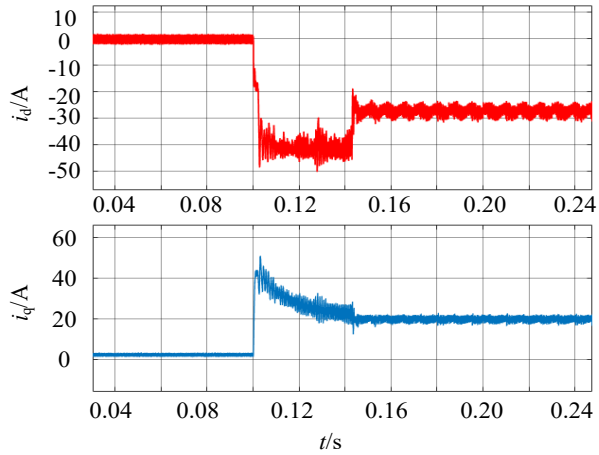

(b) Traditional control method

Fig. 10. A-axis and d-axis current response curves

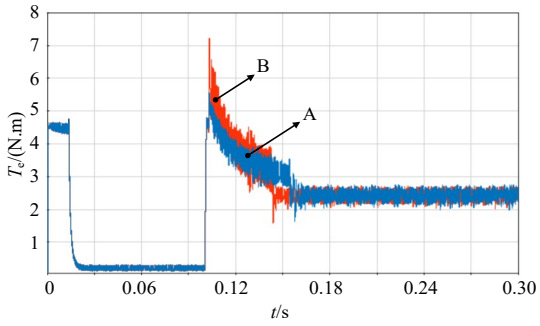

Fig. 11. Electromagnetic torque curve

Curve A and curve B are electromagnetic torque curves based on this control algorithm and traditional control algorithm respectively

As depicted in Fig. 11, with the use of the proposed control algorithm, the electromagnetic torque curve was smoother, and the average torque pulse value was smaller when the speed and load torque changed suddenly. Under the traditional control algorithm, the electromagnetic torque fluctuation was more significant, and the average torque pulse value was higher. The above result reveals that the pure electric vehicle based on the proposed control algorithm has better ride comfort when the speed and driving resistance change.

VII. Conclusion

An IPMSM fuzzy single-current field weakening control algorithm for pure electric vehicles was proposed to solve the problem that complex road conditions, irregular variation of driving speed, and adverse working conditions affect the driving motor parameters of pure electric vehicles and traditional motor control PI regulator parameters that cannot change in real time with vehicle driving requirements. The simulation model of the algorithm was built based on Matlab/Simulink, and then it was compared with the traditional PI-adjusted single-current field weakening control algorithm. The results suggested that the proposed control algorithm possessed a faster response speed in the field weakening region and reduced the a-axis and d-axis current coupling, and the system was endowed with strong anti-interference and robustness. Furthermore, the feasibility and effectiveness of the proposed control algorithm were validated.

References

[1] A Wang. A Novel PM Machine Design and Flux-weakening Control for Renewable Energy Vehicle[M]. Beijing: CHINA MACHINE PRESS, 2013: 5-6.

[2] China Government Network. Energy Saving and New Energy Automobile Industry Development Plan (2012-2020) [EB/OL]. http://www.gov.cn/, 2012-07-09.

[3] China Government Network. New Energy Automobile Industry Development Plan (2021-2035) [EB/OL]. http://www.gov.cn/, 2020-10-20.

[4] S Yang. Research on Control Strategy of High-Speed Permanent Magnet Synchronous Motor for Electric Vehicles[D].Wuhan: Hubei University of Technology, 2016.

[5] R Chen, Z.Q Deng, Y.G Yan. Application Research on Differential Feedback Control in Permanent Magnet Motor Servo System [J]. Transactions of China Electrotechnical Society, vol.20, no.9, pp. 92-97, Sep. 2005, http://doi.org/10.19595/j.cnki.1000-6753.tces.2005.09.018.

[6] G.Q Li, H.J Ge, T.X Liu. et al. Pseudo Derivative Feedback Control for PMSM Drive System [J]. Transactions of China Electrotechnical Society, vol.28, no.8, pp.18-23, Aug.2010. http://doi.org/10.19595/j.cnki.1000-6753.tces.2010.08.004

[7] W.H Wang, X Xiao. An Improved PI Regulator for Current Loop of PMSM Taking One-step-delay into Consideration [J]. Proceedings of the CSEE , vol. 34, no. 12. pp: 1882-1888, Apr. 2014. http://doi.org/10.13334/j.0258-8013.pcsee.2014.12.007

[8] W.H Wang, X Xiao, Y.S Ding. An Improved Predictive Current Control Method for Permanent Magnet Synchronous Motors [J]. Transactions of China Electrotechnical Society, vol. 28, no. 3, pp: 50-55, Mar. 2013. http://doi.org/10.19595/j.cnki.1000-6753.tces.2013.03.007

[9] J.L Miao, D.W Zheng, C.X Zhou. Direct torque control of SPMSM based on hybrid sliding mode controller and arctangent observer [J].Control and Decision, vol. 34, no. 9, pp: 1831-1839, Sep.2019, http://doi.org/10.13195/j.kzyjc.2018.1624.

[10] X Li, S Chi, C Liu, et al. Flux-Weakening Control with Single Current Regulator of Permanent Magnet Synchronous Motor Based on Virtual Resistor [J]. Transactions of China Electrotechnical Society, vol. 35, no. 5, pp: 1046-1054, Mar. 2020, http://doi.org/10.19595/j.cnki.1000-6753.tces.190689

[11] J.S Kang, F Jiang, Z.M Zhong Z, et al. Overviews of Flux Weakening Control Schemes with Permanent Magnet Synchronous Motor Used in Electric Vehicles [J]. Journal of power supply, vol. 15, no. 1, pp: 15-22, Jan. 2017, http://doi.org/10.13234/j.issn.2095-2805.2017.1.15

[12] C.Y Wang. Modern Control Technology for Electric Machines[M]. Beijing: CHINA MACHINE PRESS, 2014: 121.

[13] J.W Cui. Research on Permanent Magnet Motor and Drive Control in Electric Vehicle Application [D].Nanjing: Nanjing University of Aeronautics and Astronautics, 2015.

[14] H.Y Wu. Research of Interior Permanent Magnet Synchronous Motor Drive System for Electric Vehicle [D]. Wuhan: Huazhong University of Science and Technology, 2015.
[15] F Peng Research on Parameter Self Tuning of Permanent Magnet Synchronous Motor Control Systems [D]. Guangzhou: Guangdong University of Technology, 2016.
[16] T Englert, K. Graichen. A Fixed-Point Iteration Scheme for Model Predictive Torque Control of PMSMs[J]. IFAC-Papers on Line, vol. 51, no. 20, pp: 568-573, Nov. 2018, http://doi.org/10.1016/j.ifacol.2018.11.030.
[17] S. H Hosseini, M Tabatabaei. IPMSM Velocity and Current Control Using MTPA Based Adaptive Fractional Order Sliding Mode Controller[J]. Engineering Science and Technology, an International Journal,vol. 20, no. 3, pp: 896-908. Jun. 2017, https://doi.org/10.1016/j.jestch.2017.03.008.
[18] H Wei, J Yu, Y Zhang, et al. High-Speed Control Strategy for Permanent Magnet Synchronous Machines in Electric Vehicles Drives: Analysis of Dynamic Torque Response and Instantaneous Current Compensation[J]. Energy Reports, vol.6, pp: 2324-2335, Nov. 2020, https://doi.org/10.1016/j.egyr.2020.08.016
[19] R. S Akhil, V. P Mini, N Mayadevi, et al. Modified Flux-Weakening Control for Electric Vehicle with PMSM Drive[J]. IFAC-Papers on Line, vol. 53, no. 1, pp: 325-331, Jun. 2020, https://doi.org/10.1016/j.ifacol.2020.06.055.

Jingbo Wu was born in Luoyang, Henan Province, China, in 1979. He received PhD degree from Beijing Institute of Technology. Now, he works in Henan University of Science and Technology. His research interests include the new energy vehicle whole vehicle control and electric drive system research. The representative paper is as follows:
1. Jingbo Wu. “Flux-Weakening Fuzzy Adaptive ST-SMO Sensorless Control Algorithm for PMSM in EV”,Journal of Supercomputing, pp.10930-10949. 2022.
https://doi.org/10.1007/s11227-021-04264-8
2. Jingbo Wu. “Hybrid Pulse High-Frequency Voltage Injection Control Algorithm of Sensorless IPMSM for Vehicles", Computational Intelligence and Neuroscience, pp.1-9. 2022.
https://doi.org/10.1155/2022/4248643
3. Jingbo Wu. “An optimized sliding-mode observer control algorithm for vehicle sensor-less PMSM", The Journal of Engineering, pp.1-10. 2023.
https://doi.org/10.1049/tje2.12253